molbank

MDPI

Communication

Assembly of Sn(IV)-Porphyrin Cation Exhibiting Supramolecular Interactions of Anion···Anion and Anion···π Systems

Hee-Joon Kim

Department of Chemistry and Bioscience, Kumoh National Institute of Technology, Gumi 39177, Korea; hjk@kumoh.ac.kr; Tel.: +82-54-4787822

Abstract: *Trans*-diaqua[*meso*-tetrakis(4-pyridyl)porphyrinato]Sn(IV) dinitrate complexes were assembled in a two-dimensional manner via hydrogen bonding between aqua ligands and pyridyl substituents. Interestingly, this supramolecular assembly was accompanied by unconventional noncovalent interactions, such as anion···anion and anion···π interactions, which were confirmed by X-ray crystallographic analysis. Two nitrate anions close to 2.070 Å were constrained in a confined space surrounded by four hydrogen-bonded Sn(IV)-porphyrin cations. The nitrate anion was also 3.433 Å away from the adjacent pyrrole ring, and the dihedral angle between the two mean planes was estimated to be 7.39°. The preference of the anion···π interaction was related to the electron-deficient π-system owing to the high-valent Sn(IV) center and cationic nature of the porphyrin complex. These two unconventional noncovalent interactions played an important role in the formation of a one-dimensional array with pairs of Sn(IV)-porphyrin cation and nitrate anion.

Keywords: supramolecular assembly; anion···anion interaction; anion···π interaction

Citation: Kim, H.-J. Assembly of Sn(IV)-Porphyrin Cation Exhibiting Supramolecular Interactions of Anion···Anion and Anion···π Systems. *Molbank* **2022**, *2022*, M1454. https://doi.org/10.3390/M1454

Received: 8 September 2022
Accepted: 22 September 2022
Published: 25 September 2022

1. Introduction

The supramolecular assembly of metalloporphyrins provides valuable insights for elucidating biochemical processes and developing photoelectronic materials [1–9]. Noncovalent intermolecular interactions, such as metal–ligand coordination [10–13], hydrogen bonding [14,15], and π-stacking [16–18], have been mainly utilized in the supramolecular assembly of metalloporphyrins. Introduction of specific functional groups onto the peripheral positions enables the corresponding intermolecular interactions. In this context, Sn(IV)-porphyrin is a more attractive motif for constructing self-assembled metalloporphyrin nanostructures [19–22], because they can exhibit unique features by strongly adopting functional ligands at their axial positions [23,24]. Thus, cooperative interactions between two different functional groups in six-coordinated Sn(IV)-porphyrins have led to various assembled structures for the development of functional porphyrin materials [25–33]. Recently, nanomaterials based on the assembly of Sn(IV)-porphyrins have been intensively studied for application to visible light-sensitive photocatalysis [34–41].

Among the various types of supramolecular assemblies, ionic assemblies are accompanied by the coupling of structurally different ionic building blocks via strong electrostatic interactions [42]. The predominant driving force arises from the attractive electrostatic interaction between cation and anion species. Accordingly, anions and cations are arranged in a way that minimizes the distance between oppositely charged species, whereas electrostatic repulsion maximizes the space between like-charged species (cation···cation or anion···anion). However, certain ionic assembled structures involve unconventional interactions, indicated by the unusual proximity between like-charged species [43–45]. Moreover, these types of contacts can play an important role in the formation of specific supramolecular assemblies [46–49].

In contrast, porphyrin macrocycles are composed of well-defined and largely delocalized π-electron systems. The π-electronic nature of porphyrin molecules crucially contributes to the supramolecular assembly through π-stacking [16–18]. Owing to their electron-deficient character, cation species can attractively interact with π-electron systems, commonly known as cation···π interactions [50–52]. However, anion···π interactions are unconventional because anions and π-electron systems are expected to interact repulsively with each other due to the involvement of electron-rich entities [53,54]. In stark contrast to the mature research field regarding cation···π interaction, anion···π interaction remains a challenging area to explore in supramolecular chemistry [55].

The supramolecular assembly of an amphoteric Sn(IV)-porphyrin cation complex is reported here, in which unconventional noncovalent interactions such as anion···anion and anion···π notably occurred and played an important role in constructing a specific supramolecular array. Sn(IV)-porphyrin cation complexes exhibiting unconventional interactions of anion···anion and anion···π could provide new insights for creating elaborate ionic assemblies.

2. Results and Discussion

Trans-diaqua[*meso*-tetrakis(4-pyridyl)porphyrinato]Sn(IV) dication complex (**SnP^{2+}**) was prepared using an acid–base equilibrium reaction between *trans*-dihydroxo[*meso*-tetrakis(4-pyridyl)porphyrinato]Sn(IV) (**SnP**) [56] and *trans*-diaqua[*meso*-tetrakis(4-pyridinium)porphyrinato]Sn(IV) hexacation complex (**SnP^{6+}**) [57] (Scheme 1). **SnP** has six Lewis-base atoms from the hydroxo ligand and pyridyl substituent, whereas **SnP^{6+}** has six acidic hydrogen atoms. Accordingly, the two complementary complexes produced an amphoteric complex, **SnP^{2+}**, via the acid–base reaction.

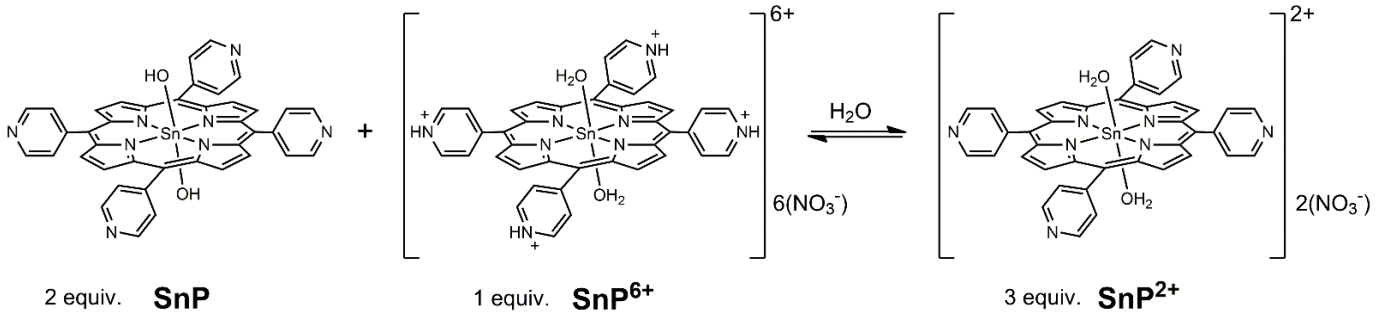

Scheme 1. Preparation of **SnP^{2+}**, and chemical structures of Sn(IV)-porphyrin complexes.

In the ESI mass spectrum, a parent ion peak appeared at m/z 753.1, which is consistent with the formula of the [**SnP^{2+}**–OH]$^+$ species (Figure S1a). A molecular ion peak corresponding to NO_3^- was also observed in the negative mode of the ESI mass spectrum (Figure S1b). In the ^{1}H NMR spectrum of **SnP^{2+}** in DMSO-d_6 (Figure S2), the resonances for the pyridyl and β-pyrrolic protons were notably shifted to a lower field compared to **SnP** ($\Delta\delta$ = 0.07 ($H_{py\text{-}\alpha}$), 0.08 ($H_{py\text{-}\beta}$), and 0.30 ($H_{pyrrole}$) ppm). However, compared to the six-valent charged analog, **SnP^{6+}**, the resonances for **SnP^{2+}** were oppositely shifted to a higher field ($\Delta\delta$ = −0.06 ($H_{py\text{-}\alpha}$), −0.11 ($H_{py\text{-}\beta}$), and −0.05 ($H_{pyrrole}$) ppm). Therefore, the ^{1}H NMR spectral feature of **SnP^{2+}** indicated that the electronic characteristics of **SnP^{2+}** were intermediate between **SnP** and **SnP^{6+}**. In the comparison of FT-IR spectra of **SnP** and **SnP^{2+}** (Figure S3), the characteristic band for the NO_3^- anion (1350 cm^{-1}) was found only in **SnP^{2+}**.

The hydrogen-bonded supramolecular assembly of **SnP** [56] and the supramolecular assembly of **SnP^{6+}** stabilized by ionic hydrogen-bonding interactions [57] were previously reported, and have been intensively studied, including X-ray crystallography. **SnP** or **SnP^{6+}** provides a unilateral component for hydrogen bonding. **SnP** and **SnP^{6+}** have hydrogen-bonding acceptors (hydroxo ligand and pyridyl substituent) and donors (aqua ligand and pyridinium substituent), respectively. Furthermore, **SnP^{2+}** can perform both

functions (aqua ligand as the donor and a pyridyl substituent as the acceptor). Therefore, the supramolecular assembly of **SnP^{2+}** based on hydrogen bonding and ionic interactions is of interest. A single crystal suitable for X-ray crystallographic analysis was obtained from the bulk as-synthesized samples. **SnP^{2+}** crystallized into a monoclinic system with a $P2_1/c$ space group. Crystallographic analysis identified three chemical species: (*i*) *trans*-diaqua[*meso*-tetrakis(4-pyridyl)porphyrinato]Sn(IV) cation, (*ii*) nitrate anion, and (*iii*) clathrate acetone molecules, which were formulated as $[Sn(OH_2)_2(TPyP)](NO_3)_2 \cdot 2$acetone.

Figure 1 shows the structure of **SnP^{2+}** cation in the crystal. The central Sn(IV) ion adopts an octahedral geometry with the porphyrin occupying the square base and the axial coordination of two aqua ligands. The Sn(IV) ion lies on an inversion center, so that the two aqua ligands lie in an exact *trans* orientation with respect to each other. The average Sn–N bond distance was estimated to be 2.091(4) Å, which was shorter than that of **SnP** (2.101(3) Å) and longer than that of **SnP^{6+}** (2.083(2) Å). The aqua ligand in **SnP^{2+}** was clearly distinguished from the hydroxo ligand coordinated to Sn(IV)-porphyrin by comparing their bond distances. The Sn–O_{aqua} bond distance of 2.093(2) Å in **SnP^{2+}** is significantly longer than the Sn–$O_{hydroxo}$ bond distance of 2.014(3) Å in **SnP**, but is similar to that of **SnP^{6+}** (2.1024(19) Å). The structural parameters related to the Sn(IV) center in **SnP^{2+}** are summarized in Table 1 and compared with those for **SnP^{6+}** and **SnP**.

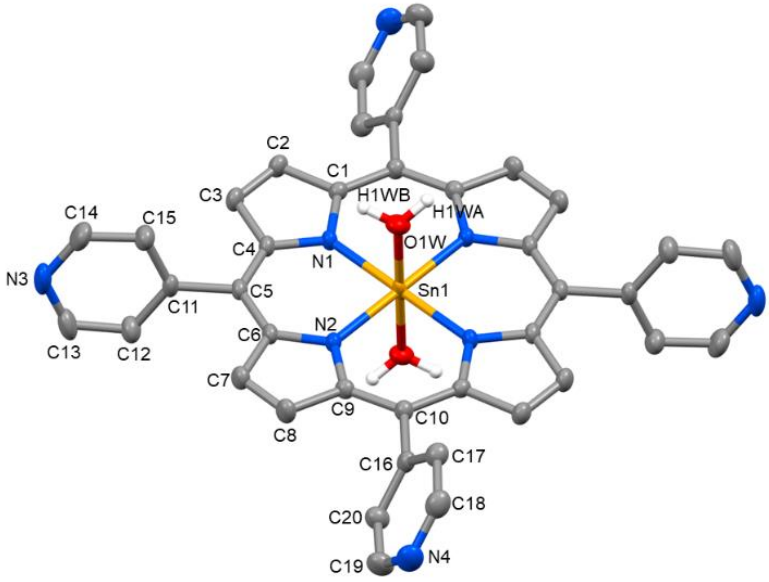

Figure 1. Molecular structure of **SnP^{2+}**. Ellipsoids were drawn at 50% probability, and hydrogen atoms of the porphyrin ligand were omitted for clarity.

Table 1. Selected bond distances (Å) and angles (°) of **SnP^{2+}** in comparison with **SnP^{6+}** and **SnP**.

	SnP^{2+}	**SnP^{6+}** [a]	**SnP** [b]
Sn–O1W	2.093(2)	2.1024(19)	2.014(3)
Sn–N1	2.093(2)	2.087(2)	2.098(3)
Sn–N2	2.089(2)	2.078(2)	2.104(3)
∠N1–Sn–N2	90.27(9)	90.52(8)	90.19(11)
∠N1–Sn–O1W	90.95(9)	89.64(8)	93.12(11)
∠N2–Sn–O1W	90.43(9)	87.56(8)	89.83(12)

Data from [a] [57] and [b] [56].

The aqua ligand of **SnP^{2+}** was hydrogen-bonded to the pyridyl nitrogen atom of an adjacent Sn(IV)-porphyrin cation, as shown in Figure 2a. The structural parameters associated with hydrogen bonding are summarized in Table 2. The distance from the aqua oxygen atom to the hydrogen-bonded pyridyl nitrogen atom was estimated to be

2.695(4) Å (O1W···N3) including 1.90 Å of H1WA···N3. The three atoms for hydrogen bonding (O1W–H1WA···N3) were arranged almost linearly at an angle of 165.2°. Thus, the Sn(IV)-porphyrin building blocks were assembled in a two-dimensional (2D) manner through hydrogen bonding between the aqua ligand and the pyridyl substituent. Figure 2b shows a hydrogen-bonded array of Sn(IV)-porphyrin cations.

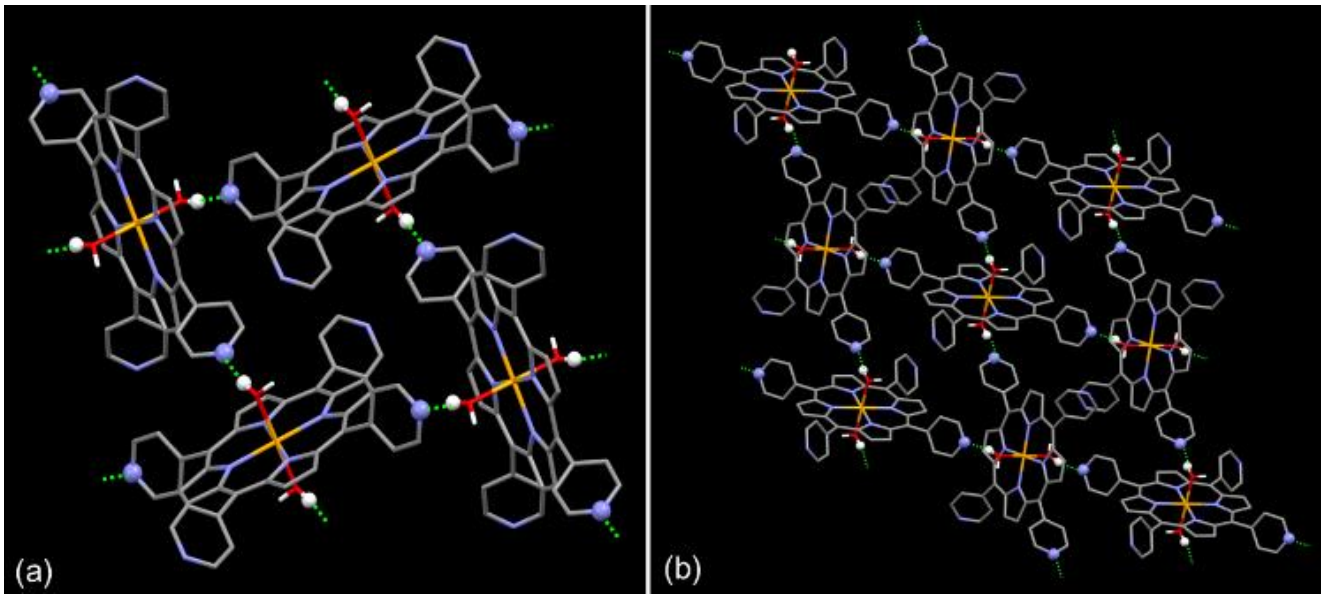

Figure 2. (**a**) Hydrogen bonds between the aqua ligands and the pyridyl substituents of **SnP^{2+}**. (**b**) The two-dimensional array of the Sn(IV)-porphyrin cations via hydrogen bonding. Hydrogen bonds are indicated by dotted lines. Hydrogen atoms of the porphyrin ligand, nitrate anions, and clathrate acetone molecules were omitted for clarity.

Table 2. Selected bond distances (Å) and angles (°) associated with hydrogen bonding (D, donor atom; A, acceptor atom).

D–H···A	*d*(D–H)	*d*(H···A)	*d*(D···A)	∠(DHA)
O1W–H1WA···N3^{i}	0.82	1.90	2.695(4)	165.2
O1W–H1WB···O2	0.82	1.81	2.610(7)	167.6
O1W–H1WB···N5	0.82	2.62	3.394(7)	157.8

Symmetry codes: (i) −x+1, y+1/2, −z+1/2.

In contrast, two nitrate anions reside in a confined space surrounded by four Sn(IV)-porphyrin cations, as shown in Figure 3a. The nitrate anion, which acts as a hydrogen-bonding acceptor, is also structurally linked with the Sn(IV)-porphyrin cation. The aqua ligand hooked the nitrate anion via hydrogen bonding in the supramolecular assembly of **SnP^{2+}** (Figure 3b). The distance from the nitrate oxygen atom to the hydrogen-bonded aqua oxygen atom is estimated to be 2.610(7) Å (O1W···O2) including 1.81 Å of H1WB···O2. The three atoms for hydrogen bonding (O1W–H1WB···O2) were arranged almost linearly at an angle of 167.6°.

More importantly, the two adjacent nitrate anions are unusually close to each other despite the repulsive forces between the same charges. The nitrate anion was 2.070 Å (O3···O3′) apart from the other nitrate anions, as shown in Figure 4a. The additional structural parameters for this contact were 2.435 Å for O3···O4′ and 2.688 Å for O3···N5′. The two nitrate anions were also coplanar with a dihedral angle of 0°. A similar unusual proximity around nitrate anions was also found in the literature [58–60], including 2.101(6) Å of the O···O distance between two nitrate anions in a lattice of {[Cd(BMIB)(H_2O)$_2$](NO_3)$_2$} (BMID = 1,4-bis(4-methyl-imidazolyl)benzene) [58]. The close contact between these two

nitrate anions means that significant anion···anion interactions have occurred. Forced contact in a confined space and stabilization by the hydrogen bond with the aqua ligand resulted in an unconventional anion···anion interaction. Unusual short distances of like-charged ions may occur because of either packing constraints or additional attractive interactions, which stabilize the crystal structure [43–45].

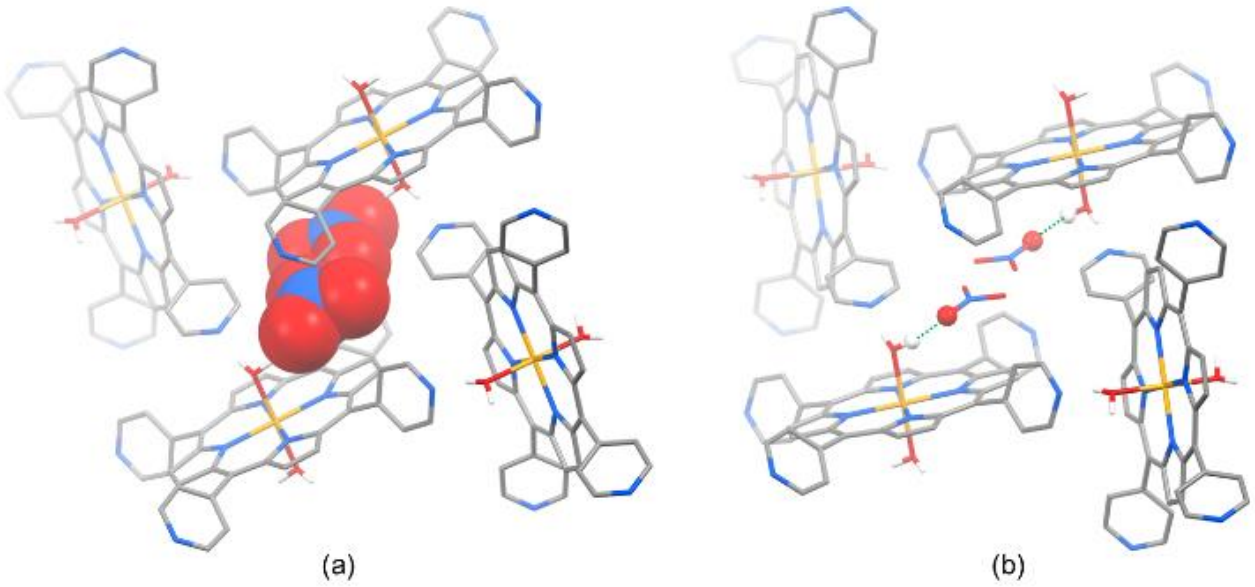

Figure 3. (**a**) Position of nitrate anions in a confined space surrounded by Sn(IV)-porphyrin cations. (**b**) Hydrogen bonds between nitrate anions and aqua ligands. Hydrogen bonds are indicated by dotted lines. Hydrogen atoms of porphyrin ligand and clathrate acetone molecules were omitted for clarity.

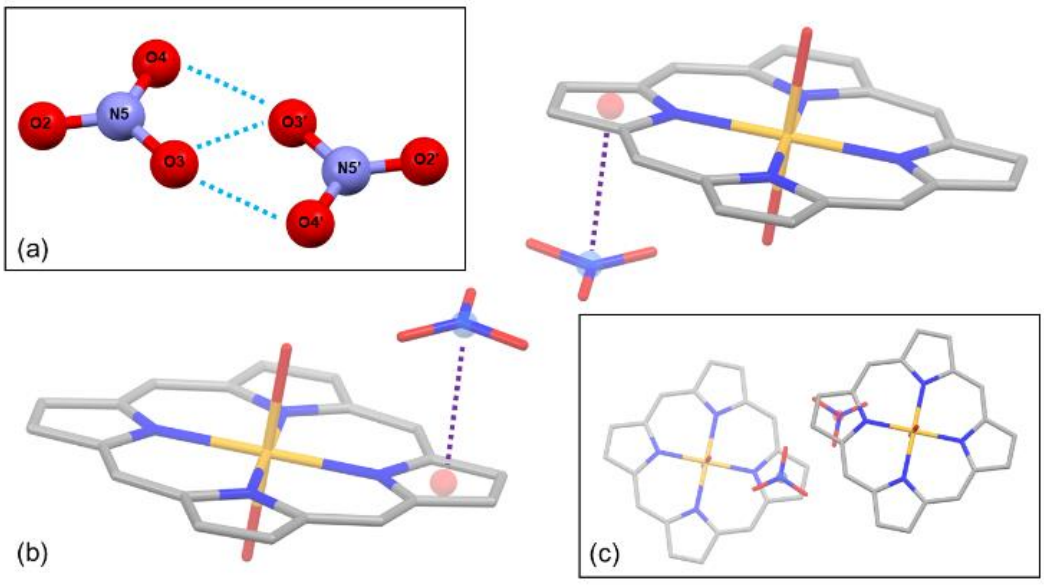

Figure 4. (**a**) Close contact between two nitrate anions. Dotted lines indicate anion···anion interactions. (**b**) Side view of the anion···π interaction indicated by dotted lines between the two centroids. (**c**) Top view along the axis connecting the two centroids. Pyridyl substituents and hydrogen atoms were omitted for clarity.

Another peculiarity is the occurrence of a nitrate···π-system of pyrrole contacts in the crystal of $\mathbf{SnP^{2+}}$ (Figure 4b,c). The centroid of the nitrate anion was 3.433 Å from

that of an adjacent pyrrole ring, and the dihedral angle between the two mean planes was estimated to be 7.39°. The high-valent Sn(IV) center and the additional cationic nature of **SnP^{2+}** made the porphyrin ligand an electron-deficient π-system. Consequently, the nitrate anion preferentially interacted with the pyrrole ring. Notably, this is a rare example of crystallographic evidence of the simultaneous occurrence of anion···anion and anion···π interactions.

The Sn(IV)-porphyrin cation and nitrate anion layers were alternately stacked to form a one-dimensional (1D) supramolecular array (Figure 5a). Given the formally repulsive nature of contact between two nitrate anions, this assembly was expected to have extremely low energy compared to a cation···anion array. However, crystal packing was partially affected by this weak interaction. Consequently, unconventional anion···anion interactions between the two nitrate anions played a critical role in forming the 1D array with pairs of Sn(IV)-porphyrin cation and nitrate anion. There were two different directions for the 1D arrays, and these 1D arrays expanded alternately, as shown in Figure 5b. In adjacent stacked 1D arrays with different orientations, Sn(IV)-porphyrins were tilted at a dihedral angle of approximately 76.6° with respect to each other.

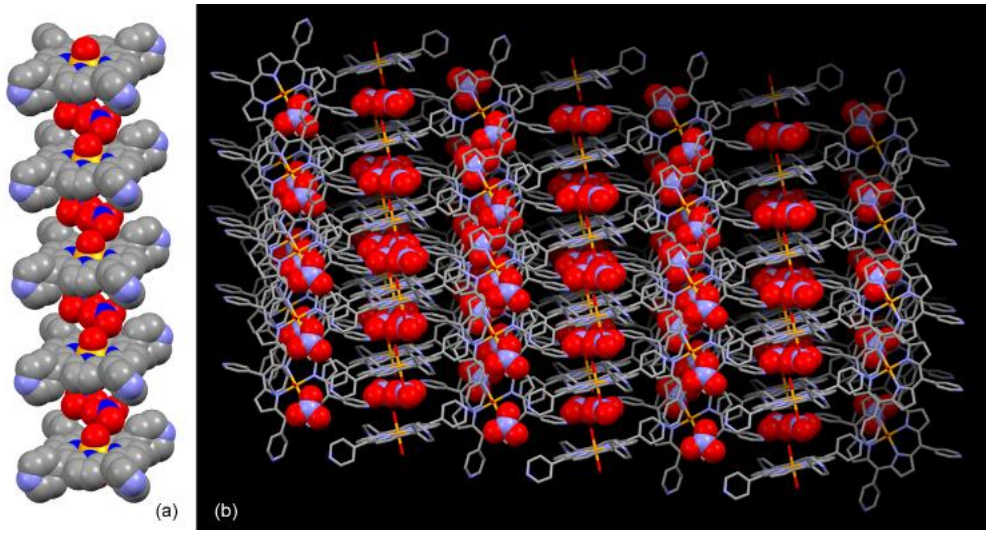

Figure 5. (**a**) Packing view of alternating layers of Sn(IV)-porphyrin cations and nitrate anions. (**b**) Perspective view of the arrays. Hydrogen atoms and clathrate acetone molecules were omitted for clarity.

3. Materials and Methods

Trans-dihydroxo[*meso*-tetrakis(4-pyridyl)porphyrinato]Sn(IV) (**SnP**) [56] and *trans*-diaqua[*meso*-tetrakis(4-pyridinium)porphyrinato]Sn(IV) (**SnP^{6+}**) hexanitrate [57] complexes were prepared using previously reported procedures. UV-vis and IR spectra were recorded using a Hewlett-Packard 8453 diode array and a Jasco FTIR-460 Plus spectrophotometer, respectively. ^{1}H NMR spectra were obtained using a Bruker BIOSPIN/AVANCE III 400 spectrometer. Electrospray ionization (ESI) mass spectra were recorded using a Waters ZQ 2000 LC/MS spectrometer. Elemental analyses were performed using a ThermoQuest EA 1110 analyzer.

3.1. Preparation of Trans-diaqua[meso-tetrakis(4-pyridyl)porphyrinato]Sn(IV) Dinitrate

Trans-dihydroxo[*meso*-tetrakis(4-pyridyl)porphyrinato]Sn(IV) (385.0 mg, 0.5 mmol) and *trans*-diaqua[*meso*-tetrakis(4-pyridinium)porphyrinato]Sn(IV) hexanitrate (287.0 mg, 0.25 mmol) were mixed in 20 mL of water. The reaction mixture was heated under reflux for 24 h and stirred at room temperature for an additional 24 h. After the acetone (100 mL) was layered over for slow diffusion, the solution was allowed to stand for a week. Block-shaped violet crystals were obtained via filtration. Yield: 86%. ^{1}H NMR (400 MHz, DMSO-d$_6$) δ

9.42 (s, 8H, $H_{pyrrole}$), 9.18 (d, J = 2.2 Hz, 8H, $H_{py\text{-}\alpha}$), 8.38 (d, J = 4.1 Hz, 8H, $H_{py\text{-}\beta}$). UV-vis (DMSO, nm): λ_{max} (log ε) 410 (4.20), 520 (3.05), 552 (3.78), and 592 (3.52). Mass (ESI): m/z 754.0 [$(M–H_2O)^+$ requires 754.13]. Elemental analysis was performed on evacuated samples. Anal. Calcd. for $C_{40}H_{28}N_{10}O_8Sn$: C, 53.65; H, 3.15; N, 15.64. Found: C, 53.23; H, 3.58; and N, 15.21.

3.2. X-ray Crystal Structure Determination

Single crystals in the as-synthesized sample were picked up using Paraton-*N* hydrocarbon oil on a glass fiber and mounted on a Bruker APEX-II CCD diffractometer equipped with a graphite monochromated Mo Kα (λ = 0.71073 Å) radiation source and a CCD detector. Data were collected at 173(2) K in a cold N_2 stream. Three sets of 15 frames of two-dimensional diffraction images were collected and processed to deduce the cell parameter and orientation matrix. All crystallographic data were corrected for Lorentz and polarization effects (SAINT) [61]. Empirical absorption correction was applied (SADABS) [62]. The integration of data using triclinic unit cell yielded 12,463 reflections, of which 4,495 were independent and greater than $2\sigma(I)$. The final cell constants were refined with 4,495 reflections at $2.059^\circ \leq \theta \leq 26.998^\circ$. Data analysis showed negligible decay during data collection. The structure was solved using direct methods and the subsequent difference Fourier syntheses and refined using the SHELXTL software package [63]. Crystallographic data and additional details of data collection and refinement are summarized in Table S1. All non-hydrogen atoms were refined anisotropically. All hydrogen atoms were included in the calculated positions, with isotropic thermal parameters 1.2 times those of the attached atoms. The final full matrix least-squares refinement of F^2 converged to R_1 = 0.0471 (all data) and wR_2 = 0.1192 ($I > 2\sigma(I)$) with GOF = 1.116.

4. Conclusions

SnP^{2+} was synthesized utilizing the acid–base reaction of Lewis bases in **SnP** and protons in **SnP^{6+}**, demonstrating that two complementary porphyrin complexes can generate an amphoteric porphyrin complex from the acid–base reaction. **SnP^{2+}** has components for hydrogen bonding, with aqua ligands and pyridyl substituents serving as the donor and acceptor, respectively. X-ray structural analysis revealed that the Sn(IV)-porphyrin building blocks were assembled in a 2D manner through hydrogen bonding between the aqua ligand and pyridyl substituent. Furthermore, the aqua ligand simultaneously interacted with the nitrate anion via hydrogen bonding in the supramolecular assembly of **SnP^{2+}**. More importantly, the unconventional anion···anion interactions of the two nitrate anions occurred in a confined space surrounded by four Sn(IV)-porphyrin cations. The anion···π-system interaction, another unconventional interaction, appeared in the proximity of the nitrate anion with the pyrrole ring. This is a rare example in which anion···anion and anion···π interactions occurred simultaneously. These findings can provide new opportunities in supramolecular chemistry, particularly for molecular hosts composed of oligomeric Sn(IV)-porphyrin with multivalent cationic charges to recognize polyanions in confined spaces.

Supplementary Materials: The following are available online: Figure S1. ESI mass spectra of **SnP^{2+}** (a) positive mode, (b) negative mode; Figure S2. ^{1}H NMR spectrum of **SnP^{2+}** in DMSO-d_6; Figure S3. Comparison of FT-IR spectra of **SnP** and **SnP^{2+}** (KBr pellet); Table S1. Crystal and structure refinement data.

Funding: This work was supported by the Kumoh National Institute of Technology (2021).

Institutional Review Board Statement: Not applicable.

Informed Consent Statement: Not applicable.

Data Availability Statement: CCDC 2173158 contains supplementary crystallographic data for this paper. These data can be obtained free of charge via http://www.ccdc.cam.ac.uk/conts/retrieving.html (or from the CCDC, 12 Union Road, Cambridge, CB2 1EZ, UK; Fax: +44 1223 336033; E-mail: deposit@ccdc.cam.ac.uk).

Acknowledgments: The author thanks Jaheon Kim for his helpful discussion.

Conflicts of Interest: The author declares no conflict of interest.

Sample Availability: Samples of the compounds are not available from the authors.

References

1. Drain, C.M.; Hupp, J.T.; Suslick, K.S.; Wasielewski, M.R.; Chen, X. A perspective on four new porphyrin-based functional materials and devices. *J. Porphyr. Phthalocyanines* **2002**, *6*, 243–258. [CrossRef]
2. Milic, T.N.; Chi, N.; Yablon, D.G.; Flynn, G.W.; Batteas, J.D.; Drain, C.M. Controlled hierarchical self-assembly and deposition of nanoscale photonic materials. *Angew. Chem. Int. Ed.* **2002**, *41*, 2117–2119. [CrossRef]
3. Suslick, K.S.; Rakow, N.A.; Kosal, M.E.; Chou, J.-H. The materials chemistry of porphyrins and metalloporphyrins. *J. Porphyr. Phthalocyanines* **2000**, *4*, 407–413. [CrossRef]
4. Chambron, J.-C.; Heitz, V.; Sauvage, J.-P. *The Porphyrin Handbook*; Kadish, K.M., Smith, K.M., Guilard, R., Eds.; Academic Press: San Diego, CA, USA, 2000; Volume 6, pp. 1–42.
5. Chou, J.-H.; Nalwa, H.S.; Kosal, M.E.; Rakow, N.A.; Suslick, K.S. Applications of Porphyrins and Metalloporphyrins to Materials Chemistry. In *The Porphyrin Handbook*; Kadish, K.M., Smith, K.M., Guilard, R., Eds.; Academic Press: San Diego, CA, 2000; Volume 6, pp. 43–131.
6. George, S.; Goldberg, I. Self-Assembly of Supramolecular Porphyrin Arrays by Hydrogen Bonding: New Structures and Reflections. *Cryst. Growth Des.* **2006**, *6*, 755–762. [CrossRef]
7. Vinodu, M.; Goldberg, I. New assembly modes of porphyrin-based networks. *CrystEngComm* **2003**, *5*, 204–207. [CrossRef]
8. Goldberg, I. Crystal engineering of porphyrin framework solids. *Chem. Commun.* **2005**, 1243–1254. [CrossRef]
9. Hasobe, T. Photo-and electro-functional self-assembled architectures of porphyrins. *Phys. Chem. Chem. Phys.* **2012**, *14*, 15975–15987. [CrossRef]
10. Northrop, B.H.; Zheng, Y.-R.; Chi, K.-W.; Stang, P.J. Self-Organization in Coordination-Driven Self-Assembly. *Acc. Chem. Res.* **2009**, *42*, 1554–1563. [CrossRef]
11. Horike, S.; Shimomura, S.; Kitagawa, S. Soft porous crystals. *Nat. Chem.* **2009**, *1*, 695–704. [CrossRef]
12. Farha, O.K.; Shultz, A.M.; Sarjeant, A.A.; Nguyen, S.T.; Hupp, J.T. Active-Site-Accessible, Porphyrinic Metal-Organic Framework Materials. *J. Am. Chem. Soc.* **2011**, *133*, 5652–5655. [CrossRef]
13. Lee, C.Y.; Farha, O.K.; Hong, B.J.; Sarjeant, A.A.; Nguyen, S.T.; Hupp, J.T. Light-Harvesting Metal-Organic Frameworks (MOFs): Efficient Strut-to-Strut Energy Transfer in Bodipy and Porphyrin-Based MOFs. *J. Am. Chem. Soc.* **2011**, *133*, 15858–15861. [CrossRef]
14. Würthner, F.; Kaiser, T.E.; Saha-Möller, C.R. J-Aggregates: From Serendipitous Discovery to Supramolecular Engineering of Functional Dye Materials. *Angew. Chem. Int. Ed.* **2011**, *50*, 3376–3410. [CrossRef]
15. Madueno, R.; Raisanen, M.T.; Silien, C.; Buck, M. Functionalizing hydrogen-bonded surface networks with self-assembled monolayers. *Nature* **2008**, *454*, 618–621. [CrossRef]
16. Watson, M.D.; Fechtenkotter, A.; Müllen, K. Big Is Beautiful-"Aromaticity" Revisited from the Viewpoint of Macromolecular and Supramolecular Benzene Chemistry. *Chem. Rev.* **2001**, *101*, 1267–1300. [CrossRef]
17. Hunter, C.A.; Sanders, J.K.M. The nature of .Pi.-.Pi. Interactions. *J. Am. Chem. Soc.* **1990**, *112*, 5525–5534. [CrossRef]
18. Zang, L.; Che, Y.; Moore, J.S. One-Dimensional Self-Assembly of Planar π-Conjugated Molecules: Adaptable Building Blocks for Organic Nanodevices. *Acc. Chem. Res.* **2008**, *41*, 1596–1608. [CrossRef]
19. Medforth, C.J.; Wang, Z.; Martin, K.E.; Song, Y.; Jacobsen, J.L.; Shelnutt, J.A. Self-assembled porphyrin nanostructures. *Chem. Commun.* **2009**, 7261–7277. [CrossRef] [PubMed]
20. Kim, H.-J.; Jo, H.J.; Kim, J.; Kim, S.-Y.; Kim, D.; Kim, K. Supramolecular self-assembly of tin(IV) porphyrin channels stabilizing single-file chains of water molecules. *CrystEngComm* **2005**, *7*, 417–420. [CrossRef]
21. Shee, N.K.; Lee, C.-J.; Kim, H.-J. Hexacoordinated Sn(IV) porphyrin-based square-grid frameworks exhibiting selective uptake of CO_2 over N_2. *Bull. Korean Chem. Soc.* **2022**, *43*, 103–109. [CrossRef]
22. Shee, N.K.; Jo, H.J.; Kim, H.-J. Coordination framework materials fabricated by the self-assembly of Sn(IV) porphyrins with Ag(I) ions for the photocatalytic degradation of organic dyes in wastewater. *Inorg. Chem. Front.* **2022**, *9*, 1270–1280. [CrossRef]
23. Arnold, D.P.; Blok, J. The coordination chemistry of tin porphyrin complexes. *Coord. Chem. Rev.* **2004**, *248*, 299–319. [CrossRef]
24. Sanders, J.K.M.; Bampos, N.; Clyde-Watson, Z.; Darling, S.L.; Hawley, J.C.; Kim, H.-J.; Mak, C.C.; Webb, S.J. *The Porphyrin Handbook*; Kadish, K.M., Smith, K.M., Guilard, R., Eds.; Academic Press: San Diego, CA, USA, 2000; Volume 3, pp. 1–48.
25. Kim, H.-J.; Bampos, N.; Sanders, J.K.M. Assembly of Dynamic Heterometallic Oligoporphyrins Using Cooperative Zinc-Nitrogen, Ruthenium-Nitrogen, and Tin-Oxygen Coordination. J. *Am. Chem. Soc.* **1999**, *121*, 8120–8121. [CrossRef]

26. Kim, H.J.; Park, K.-M.; Ahn, T.K.; Kim, S.K.; Kim, K.S.; Kim, D.; Kim, H.-J. Novel fullerene–porphyrin–fullerene triad linked by metal axial coordination: Synthesis, X-ray crystal structure, and spectroscopic characterizations of *trans*-bis([60]fullerenoacetato)tin(iv) porphyrin. *Chem. Commun.* **2004**, *22*, 2594–2595. [CrossRef] [PubMed]
27. Kim, H.J.; Jeon, W.S.; Lim, J.H.; Hong, C.S.; Kim, H.-J. Synthesis, X-ray crystal structure, and electrochemistry of trans-bis(ferrocenecarboxylato)(tetraphenylporphyrinato)tin(IV). *Polyhedron* **2007**, *26*, 2517–2522. [CrossRef]
28. Kim, H.J.; Jang, J.H.; Choi, H.; Lee, T.; Ko, J.; Yoon, M.; Kim, H.-J. Photoregulated Fluorescence Switching in Axially Coordinated Tin(IV) Porphyrinic Dithienylethene. *Inorg. Chem.* **2008**, *47*, 2411–2415. [CrossRef]
29. Kim, S.H.; Kim, H.; Kim, K.; Kim, H.-J. The first tin(IV) porphyrin complex with chiral amino acid ligands: Synthesis, characterization and X-ray crystal structure of trans-bis(L-prolinato)[5,10,15,20-tetrakis-(4-pyridyl)porphyrinato]tin(IV). *J. Porphyrins Phthalocyanines* **2009**, *13*, 805–810. [CrossRef]
30. Singh, A.P.; Park, B.B.; Kim, H.-J. Facile C-C bond cleavage of β-diketones by tin(IV) porphyrin complex. *Tetrahedron Lett.* **2012**, *53*, 6456–6459. [CrossRef]
31. Kim, H.J.; Shee, N.K.; Park, K.-M.; Kim, H.-J. Assembly and X-ray crystal structures of heterometallic multiporphyrins with complementary coordination between ruthenium (II) and tin (IV) porphyrins. *Inorg. Chim. Acta* **2019**, *488*, 1–7. [CrossRef]
32. Shee, N.K.; Kim, M.K.; Kim, H.-J. Fluorescent chemosensing for aromatic compounds by supramolecular complex composed of tin(IV) porphyrin, viologen, and cucurbit[8]uril. *Chem. Commun.* **2019**, *55*, 10575–10578. [CrossRef]
33. Kim, M.K.; Shee, N.K.; Lee, J.; Yoon, M.; Kim, H.-J. Photoinduced Electron Transfer upon Supramolecular Complexation of (Porphyrinato) Sn-Viologen with Cucurbit [7] uril. *Photochem. Photobiol. Sci.* **2019**, *18*, 1996–2002. [CrossRef]
34. Shee, N.K.; Kim, M.K.; Kim, H.-J. Supramolecular Porphyrin Nanostructures Based on Coordination-Driven Self-Assembly and Their Visible Light Catalytic Degradation of Methylene Blue Dye. *Nanomaterials* **2020**, *10*, 2314. [CrossRef] [PubMed]
35. Shee, N.K.; Kim, H.-J. Self-Assembled Nanomaterials Based on Complementary Sn(IV) and Zn(II)-Porphyrins, and Their Photocatalytic Degradation for Rhodamine B Dye. *Molecules* **2021**, *26*, 3598. [CrossRef] [PubMed]
36. Shee, N.K. Kim, H.-J. Three Isomeric Zn(II)-Sn(IV)-Zn(II) Porphyrin-Triad-Based Supramolecular Nanoarchitectures for the Morphology-Dependent Photocatalytic Degradation of Methyl Orange. *ACS Omega* **2022**, *7*, 9775–9784. [CrossRef] [PubMed]
37. Jang, J.H.; Jeon, K.-S.; Oh, S.; Kim, H.-J.; Asahi, T.; Masuhara, H.; Yoon, M. Synthesis of Sn-porphyrin-intercalated trititanate nanofibers: Optoelectronic properties and photocatalytic activities. *Chem. Mater.* **2007**, *19*, 1984–1991. [CrossRef]
38. Kim, W.; Park, J.; Jo, H.J.; Kim, H.-J.; Choi, W. Visible light photocatalysts based on homogeneous and heterogenized tin porphyrins. J. *Phys. Chem. C* **2008**, *112*, 491–499. [CrossRef]
39. Kim, W.; Tachikawa, T.; Majima, T.; Li, C.; Kim, H.-J.; Choi, W. Tin-porphyrin sensitized TiO_2 for the production of H_2 under visible light. *Energy Environ. Sci.* **2010**, *3*, 1789–1795. [CrossRef]
40. Kim, H.; Kim, W.; Mackeyev, Y.; Lee, G.-S.; Kim, H.-J.; Tachikawa, T.; Hong, S.; Lee, S.; Kim, J.; Wilson, L.J.; et al. Selective oxidative degradation of organic pollutants by singlet oxygen-mediated photosensitization: Tin porphyrin versus C_{60} aminofullerene systems. *Environ. Sci. Tech.* **2012**, *46*, 9606–9613. [CrossRef]
41. Li, C.; Park, K.-M.; Kim, H.-J. Ionic assembled hybrid nanoparticle consisting of tin(IV) porphyrin cations and polyoxomolybdate anions, and photocatalytic hydrogen production by its visible light sensitization. *Inorg. Chem. Commun.* **2015**, *60*, 8–11. [CrossRef]
42. Faul, C.F.J.; Antonietti, M. Ionic self-assembly: Facile synthesis of supramolecular materials. *Adv. Mater.* **2003**, *15*, 673–683. [CrossRef]
43. He, Q.; Tu, P.; Sessler, J.L. Supramolecular Chemistry of Anionic Dimers, Trimers, Tetramers and Clusters. *Chem.* **2018**, *4*, 46–93. [CrossRef]
44. Nelyubina, Y.V.; Antipin, M.Y.; Lyssenko, K.A. Anion–anion interactions: Their nature, energy and role in crystal formation. *Russ. Chem. Rev.* **2010**, *79*, 167–187. [CrossRef]
45. Dance, I.; Scudder, M. Supramolecular Motifs: Concerted Multiple Phenyl Embraces between Ph_4P^+ Cations are Attractive and Ubiquitous. *Chem.-Eur. J.* **1996**, *2*, 481–486. [CrossRef] [PubMed]
46. Chesman, A.S.R.; Hodgson, J.L.; Izgorodina, E.I.; Urbatsch, A.; Turner, D.R.; Deacon, G.B.; Batten, S.R. Anion-anion interactions in the crystal packing of functionalized methanide anions: An experimental and computational study. *Cryst. Growth Des.* **2014**, *14*, 1922–1932. [CrossRef]
47. Wysokiński, R.; Zierkiewicz, W.; Michalczyk, M.; Scheiner, S. Crystallographic and theoretical evidences of anion···anion interaction. *ChemPhysChem* **2021**, *22*, 818–821. [CrossRef]
48. Nelyubina, Y.V.; Lyssenko, K.A.; Golovanov, D.G.; Antipin, M.Y. $NO_3^-\cdots NO_3^-$ and $NO_3^-\cdots\pi$ interactions in the crystal of urea nitrate. *CrystEngComm* **2007**, *9*, 991–996. [CrossRef]
49. Khan, S.; Roy, S.; Harms, K.; Bauzá, A.; Frontera, A.; Chattopadhyay, S. Observation of an anion···anion interaction in a square planar copper(II) Schiff base complex: DFT study and CSD analysis. *Inorg. Chim. Acta* **2019**, *487*, 465–472. [CrossRef]
50. Dougherty, D.A. Cation-pi interactions in chemistry and biology: A new view of benzene, Phe, Tyr, and Trp. *Science* **1996**, *271*, 163–168. [CrossRef]
51. Ma, J.C.; Dougherty, D.A. The Cation-π Interaction. *Chem. Rev.* **1997**, *97*, 1303–1324. [CrossRef]
52. Sussman, J.L.; Harel, M.; Frolow, F.; Oefner, C.; Goldman, A.; Tolker, L.; Silman, I. Atomic structure of acetylcholinesterase from Torpedo californica: A prototypic acetylcholine-binding protein. *Science* **1991**, *253*, 872–879. [CrossRef]
53. Quiñonero, D.; Garau, C.; Rotger, C.; Frontera, A.; Ballester, P.; Costa, A.; Deyà, P.M. Anion-π Interactions: Do They Exist? *Angew. Chem.* **2002**, *114*, 3539–3542. [CrossRef]

54. Schottel, B.L.; Chifotides, H.T.; Dunbar, K.R. Anion-π Interactions. *Chem. Soc. Rev.* **2008**, *37*, 68–83. [CrossRef] [PubMed]
55. Wang, D.-X.; Wang, M.-X. Exploring Anion-π Interactions and Their Applications in Supramolecular Chemistry. *Acc. Chem. Res.* **2020**, *53*, 1364–1380. [CrossRef] [PubMed]
56. Jo, H.J.; Jung, S.H.; Kim, H.-J. Synthesis and Hydrogen-Bonded Supramolecular Assembly of *trans*-Dihydroxotin(IV) Tetrapyridylporphyrin Complexes. *Bull. Korean Chem. Soc.* **2004**, *25*, 1869–1873.
57. Jo, H.J.; Kim, S.H.; Kim, H.-J. Supramolecular Assembly of Tin(IV) Porphyrin Cations Stabilized by Ionic Hydrogen-Bonding Interactions. *Bull. Korean Chem. Soc.* **2015**, *36*, 2348–2351. [CrossRef]
58. Tan, X.-W.; Li, H.-F.; Li, C.-H. Syntheses, Crystal Structures and Fluorescence Properties of Two Complexes Constructed from Rigid 1,4-bis(4-methyl-imidazolyl)Benzene. *Chin. J. Inorg. Chem.* **2017**, *33*, 156–162.
59. Ni, T.-J.; Yuan, Q.-T.; Zhang, W.; Yang, Z.-J.; Yu, H.-H.; Cai, H.-R. Influence of Solvents on the Formation of Silver(I) Complexes with the Flexible 1,3,5-Tris(triazol-1-ylmethyl)-2,4,6-trimethylbenzene. *Chin. J. Inorg. Chem.* **2017**, *33*, 2177–2185.
60. Bar, A.K.; Raghothoma, S.; Moon, D.; Mukherjee, P.S. Three-Component Self-Assembly of a Series of Triply Interlocked Pd_{12} Coordination Prisms and Their Non-Interlocked Pd_6 Analogues. *Chem. Eur. J.* **2012**, *18*, 3199–3209. [CrossRef]
61. *Area Detector Control and Integration Software*, Version 6.22; Bruker AXS Inc.: Madison, WI, USA, 1996.
62. Sheldrick, G.M. *SADABS: Empirical Absorption and Correction Software*; University of Gottingen: Gottingen, Germany, 1999.
63. *Program for Solution and Refinement of Crystal Structures*, Version 6.10; Bruker AXS Inc.: Madison, WI, USA, 2000.